Carbon Nanotube-Based Nanomechanical Sensor: Theoretical Analysis of Mechanical and Vibrational Properties

Toshiaki Natsuki [1,2,*]

1 Faculty of Textile Science and Technology, Shinshu University, 3-15-1 Tokida, Ueda-shi 386-8567, Japan
2 Institute of Carbon Science and Technology, Shinshu University, 4-17-1 Wakasato, Nagano 380-8553, Japan

Abstract: This paper reviews the recent research of carbon nanotubes (CNTs) used as nanomechanical sensing elements based mainly on theoretical models. CNTs have demonstrated considerable potential as nanomechanical mass sensor and atomic force microscope (AFM) tips. The mechanical and vibrational characteristics of CNTs are introduced to the readers. The effects of main parameters of CNTs, such as dimensions, layer number, and boundary conditions on the performance characteristics are investigated and discussed. It is hoped that this review provides knowledge on the application of CNTs as nanomechanical sensors and computational methods for predicting their properties. Their theoretical studies based on the mechanical properties such as buckling strength and vibration frequency would give a useful reference for designing CNTs as nanomechanical mass sensor and AFM probes.

Keywords: carbon nanotube; nanomechanical sensor; vibration; beam theory; nonlocal elasticity

1. Introduction

Since the discovery of carbon nanotubes (CNTs) in 1991 by Iijima [1], they have been recognized as one of the most promising nanomaterials and attracted great interest among researchers around the world because of the superior mechanical and physical properties. CNTs have diverse applications in various fields of science and engineering, such as electrical and electronic components, materials engineering, nano-sensor, energy storage and environment [2–6]. Many studies have revealed that the Young's modulus of single-walled CNTs (SWCNTs) were about 1 TPa and multi-walled CNTs (MWCNTs) were tested to have a tensile strength ranged from 11 to 63 GPa, which are stronger and stiffer than any known substance [7–9]. Wei et al [10] reported that CNTs could carry high current densities up to 10^9–10^{10} A/cm^2 and remained stable for extended periods of time at high temperature. CNTs are the smallest scale nanomaterials that can be observed only by a transmission electron microscope (TEM). The excellent structural characteristics and the mechanical and physical properties make CNTs potential candidates for the next generation of nanoelectromechanical systems (NEMS) [11–15].

At present, many methods have been developed to synthesize CNTs, including arc-discharge, laser ablation, and chemical processes [16,17]. Chemical vapor deposition (CVD) is the most common chemical method, and is widely used for fabricating CNTs. This method is capable of controlling growth directions on a substrate and synthesizing a large quantity of carbon nanotubes. In the experimental operation, it is very difficult to operate and control a single CNT because of an extremely small size. Since the advanced CVD technology was developed, the CVD synthesis allowed CNT growth directly on desired substrates, and growth in a variety of forms such as powders or films, aligned or coiled, including to control the diameter and length of CNTs. New electronic products and the developments can be expected based on the fabrication and characterization of novel nano

carbon materials. Many studies on using CNTs as high-frequency circuit elements, rotary actuators, nanosensors, transistors, etc. have been reported up to now [18–22]. Specifically, in CNT-based resonators, the state-of-the-art highest mass sensing resolution was achieved by using CNTs as the resonating mass detector [23].

Research and development on application of CNTs used in nanosensors is now an important subject for nano measurement. As shown in Figure 1, the research of NEMS is a collection of various technologies that include nano-materials and micro/nano processing, nanomechanics and nanoelectronic devices, and computational simulation and analysis. With the enormous development of NEMS based nanosensors, the miniaturization and integration of electronic elements can be realized using structural design and manufacturing processes. Thus, nano-force and mass measurement become possible, using resonant nanosensor based systems.
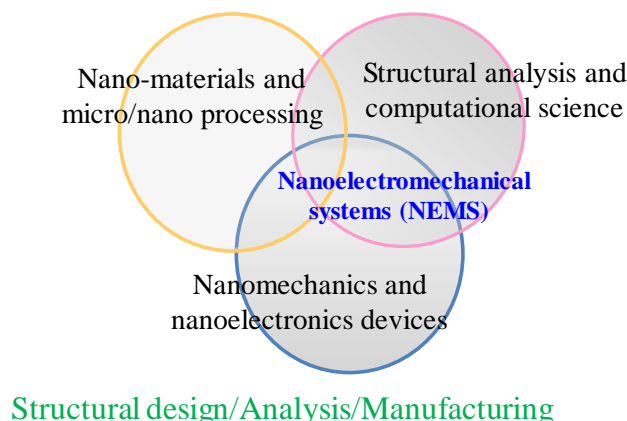
Figure 1. Components of nanoelectromechanical system.

At present, many studies on the nanomechanical sensors using CNTs and their various applications have been reported. In the review, we focus on the design of CNT-based sensors including the nano-mass sensor and the sensor used as probe for atomic force microscope (AFM), especially on the studies of their working mechanisms based on the available theoretical model.

2. CNT-Based Mass Sensor

2.1. Background of Nanomechanical Sensor Research

Conventionally, silicon based materials can be used for detecting a tiny amount of mass at the nano-level. Professor Roukes of the California Institute of Technology (Caltech) and his colleagues used silicon carbide beam for the nanomechanical resonator and made it possible to measure the minimum mass at zeptogram (10^{-21} g) level [24]. Ten years ago, the Caltech research group developed a mass sensor by using silicon instead of silicon carbide, and achieved its high mass resolution with attogram (10^{-18} g) sensitivity [25]. The new device was developed, essentially in the same way as the previous, but its smaller size and higher resonant frequency gave it a greater sensitively to added mass. In their research, the device consisted of a nanomechanical resonator with tiny silicon or silicon carbide beams about a micron long and 100 nm wide. The flat beam was clamped at both ends, and set oscillating at a frequency of 100 MHz or more. The principle of mass detection is based on frequency shift when a tiny mass is attached to the beam. In the mechanical mass sensor consisting of silicon beam, it is important to know the sensitivity of vibration frequency shift for the attached nanomass. However, since the CNTs have very small diameter, higher stiffness and strength than silicon or silicon dioxide, the CNT-based resonator can maintain high resonance frequencies to measure extremely tiny mass. The group of Professor Heer (Georgia Institute of Technology) initially proposed an idea of using a single CNT as highly sensitive nanobalances [26]. As shown in Figure 2, they succeeded in attaching

a carbon particle to the end of a nanotube and setting the nanotube to a special electron microscope stage. The methods developed were well studied to measure masses in the picogram-to-femtogram range. The mass of this nanoparticle was determined from the resonance frequency shift of a CNT nanocantilever under a transmission electron microscope (TEM) after the mass was attached to the tip of the CNT, and was measured to be about 22 fg (Femtogram: 10^{-15} g) [26,27].
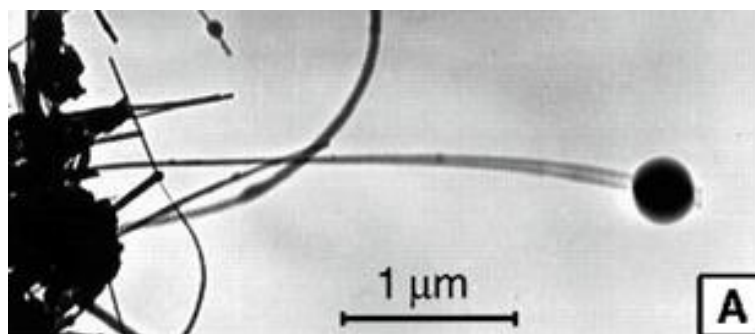

Figure 2. Resonance vibrations of a nanotube loaded with a carbon nanoparticle. Adapted with permission from [26], Copyright AAAS, 1999.

Subsequently, the research on an atomic-resolution nanomechanical mass sensor that can measure atomic mass level was reported [28]. Figure 3 shows the entire nanomechanical mass spectrometer apparatus. A TEM image of a nanomechanical mass spectrometer device constructed from a double-walled CNT (DWCNT) is shown in Figure 3a. The nanotube device was placed at one end of an ultra-high vacuum (UHV) chamber as shown in Figure 3b. In the UHV chamber, gold atoms were evaporated from a tungsten filament away from the nanotube device. To control the number of loaded atoms onto the device, a shutter was inserted between the evaporation source and the nanotube to interrupt the gold mass loading. A water-cooled quartz crystal microbalance (QCM) provided an alternate means of calibrating the system through measurement of mass flux. Figure 3c shows a schematic of the nanomechanical resonance detection circuit, which was used to measure the resonant frequency of the nanotubes. The detection technique was based on a nanotube radio receiver design and relied on the unique field emission properties of CNTs. There existed a strong coupling between the field emission current from CNTs and their mechanical vibrations. Briefly, an amplitude modulated (AM), sweep generator were coupled to the nanotube, via a voltage-controlled oscillator (VCO), RF signal, forcing it to resonate, and consequently modulating the field emission current. The modulated field emission current was recovered by a lock-in amplifier and the resonance peak was detected.

Li and Zhu [29] proposed an optical detection technique for weighing a single-atom by using surface plasmon and CNT resonator. The mass of a single atom could be determined by vibrational frequency shift of CNTs while the atom attached to the nanotube surface. Figure 4 shows schematic of a mass sensor based on a doubly clamped CNT illuminated by a strong pump beam and a weak signal beam. A single gold metal nanoparticle (MNP) was attached to the tip of a sharp optical fiber and positioned at a distance R away from the CNT. Moreover, a single xenon atom was deposited onto the CNT surface. The inset of Figure 4 shows the energy levels of a localized exciton in CNTs while dressing the surface plasmon and the vibration of the CNT. AFM was used to probe the tip and stabilize its distance to the CNT [30,31]. The mass of atoms attached to the CNT surface could be measured conveniently and precisely through frequency shift in the absorption spectrum. Owing to the ultralight mass and higher stiffness of the CNT, and spectral enhancement by using surface plasmon, this method resulted in a narrow linewidth with kHz and higher sensitivity, which was more sensitive than traditional electromechanical mass detection techniques. Especially, heating and energy loss characteristics for electrical detection could be avoided in all-optical technique.
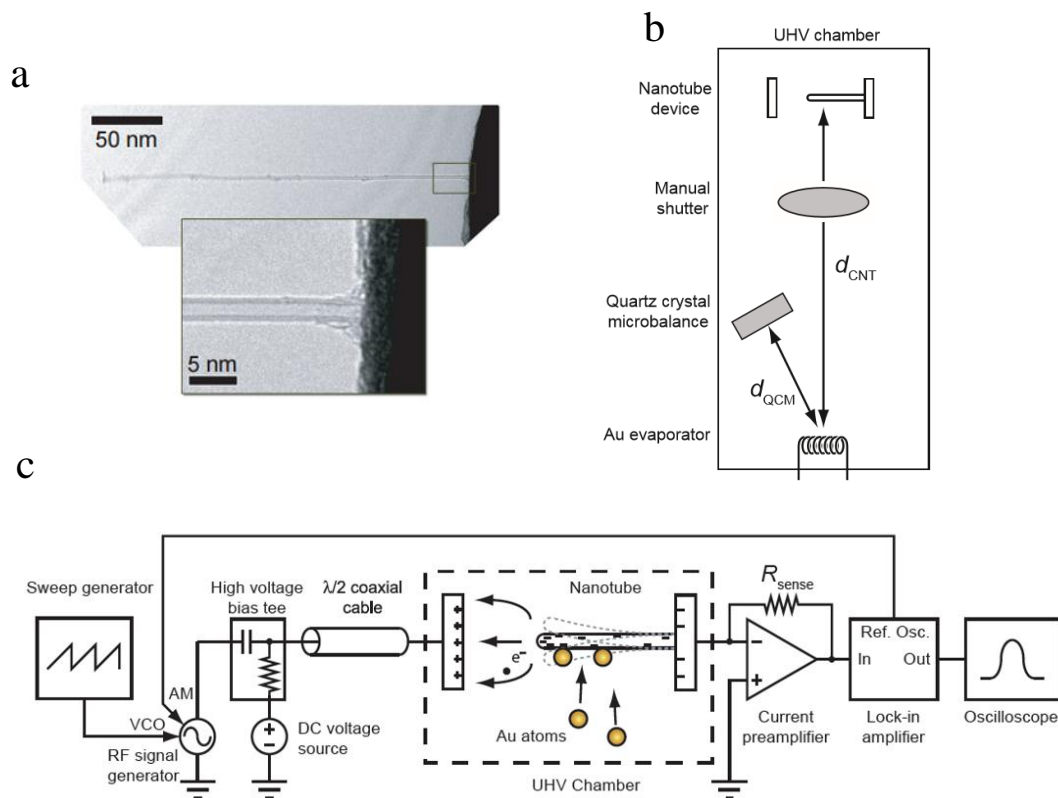
Figure 3. Nanomechanical mass spectrometer device and schematics. (**a**) TEM image of a nanomechanical mass spectrometer device constructed from a double-walled CNT (DWCNT), (**b**) The nanotube device was placed at one end of an ultra-high vacuum (UHV) chamber, (**c**) Schematic of the nanomechanical resonance detection circuit. Adapted with permission from [28], Copyright Nature Publishing Group, 2008.
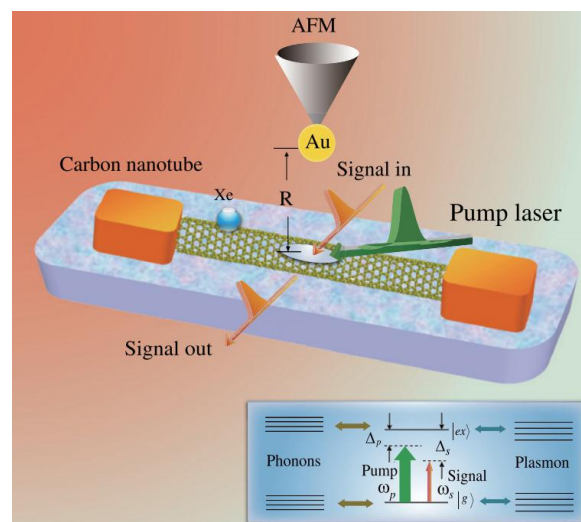

Figure 4. Schematic of a mass sensor based on a doubly clamped carbon nanotube. Adapted with permission from [29], Copyright IOP, 2012.

Lassagne et al. [32] used extremely tiny CNT with 1 nm diameter as a nanomechanical resonator for mass sensing. The performances, which were tested by measuring the mass of evaporated chromium atoms, were exceptional. Figure 5 shows diagrams of (a) experimental setup and (b)

the measurement circuitry. Nanomechanical CNT resonators were fabricated by means of standard nanofabrication techniques, and nanomass sensing experiments were carried out by evaporating chromium atoms onto the CNT resonators. As shown in Figure 5b, to track the high-frequency charge modulation, a mixing technique was employed by applying voltage $V_g^{ac} \cos(2\pi f t)$ on the gate and $V_{SD} \cos[2\pi(f + \delta f)t]$ on the source. Based on measurement of a mixing current I_{mix} on the drain at frequency change δf, the shifts of resonance frequency were obtained as a function of the deposited mass. The results found that the mass responsivity was 11 Hz/yg (1 yg $= 10^{-24}$ g) and the mass resolution is 25 zg (1 zg $= 10^{-21}$ g) at room temperature. When the CNT was cooled down to 5 K in a cryostat, the mass resolution increased and corresponded to a resolution of 1.4 zg because the signal for the detection of mechanical vibrations was improved.
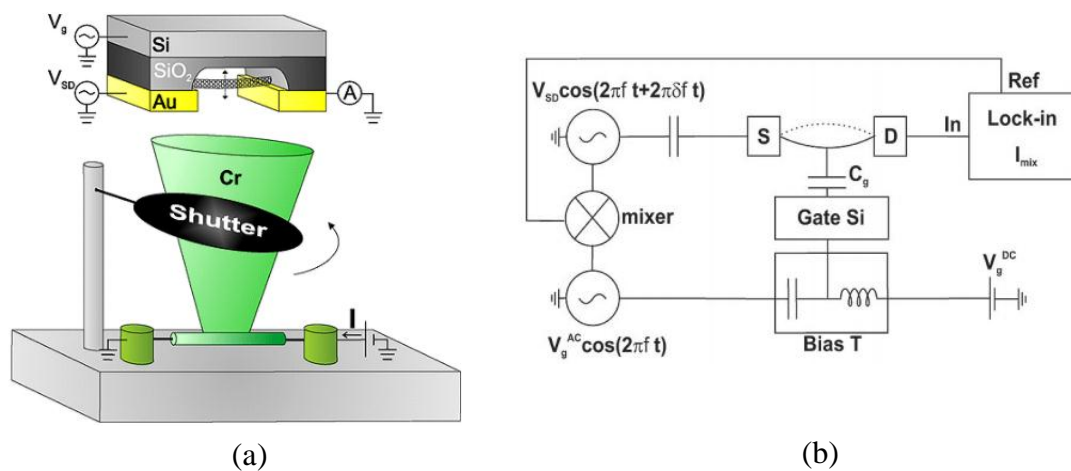

(a)   (b)

Figure 5. Schematics of the experimental setup and the measurement circuitry. Adapted with permission from [32], Copyright ACS, 2008.

2.2. Theoretical Approach of Vibration Characteristics

As described above, the detection principle of a CNT-based mass sensor is based on the fact that the resonant frequency is sensitive to the resonator mass, which includes the mass of the resonator itself and the mass attached on the CNT resonator. A change in the resonant frequency occurs when an additional mass is attached on the resonator. However, one of main problems on mass detection is how to accurately quantify the tiny change in the resonant frequency due to the added mass. Some theoretical investigation, such as the molecular dynamics (MD) method and continuum mechanics, on mass sensing characteristics has been reported so far. Although MD is widely used in nanomaterial science and is a good method for analyzing properties of CNT structure, the requested computational power is limited to a fast computer with a high capacity hard disk. Moreover, the analysis using the MD method is a cost-intensive and time-consuming process. In response to the issues, well established continuum mechanics model on a nanoscale is a challenging task. At present, the continuum mechanics has been successfully used to simulate static and dynamic properties of carbon nanotubes [33–36].

The research group of Prof. Chou [37] reported initially that the CNT resonators were assumed to be either cantilevered or bridged and were simulated based on the molecular structural mechanics method. In the research, the fundamental frequency of the CNT was obtained by simulating a SWCNT as an equivalent space frame-like structure and solving the motion equation of the system. For free vibration of the nanotube in its fundamental modes, the governing equation of motions was given by:

$$[M]\{\ddot{y}\} + [K]\{y\} = \{0\}, \tag{1}$$

where $[M]$ and $[K]$ were the global mass and stiffness matrices, respectively, and $\{\ddot{y}\}$ and $\{y\}$ were the nodal displacement vector and acceleration vector, respectively. After condensation of the mass and

stiffness matrices, applying the static condensation method, the fundamental frequencies and mode shapes were obtained from the solution of the eigenproblem

$$\left([K]_s - \omega^2 [M]_s\right)\{y_p\} = \{0\}, \tag{2}$$

where $[K]_s$ and $[M]_s$ were the condensed stiffness matrix and mass matrix, respectively. $\{y_p\}$ was the displacement of carbon atoms, and $\omega(\omega = 2\pi f)$ was the angular frequency.

Based on the method of molecular structural mechanics, the changes in resonant frequency due to the attached mass were calculated. Figure 6 shows the variation of frequency shift with the attached mass on the cantilevered nanotube resonators. The frequency shifts were defined as the difference between the fundamental frequencies of a nanotube with and without attached mass. The effects of length and diameter of CNTs on the frequency shifts were investigated in detail. It was clear that the frequency shift increased with the increase of attached mass, and the sensitivity of resonant frequency shifts to both tube length and diameter had been demonstrated. The mass sensitivity of CNT-based nanobalances could reach 10^{-21} g, and a logarithmically linear relationship existed between the resonant frequency and the attached mass when the mass was larger than 10^{-20} g.
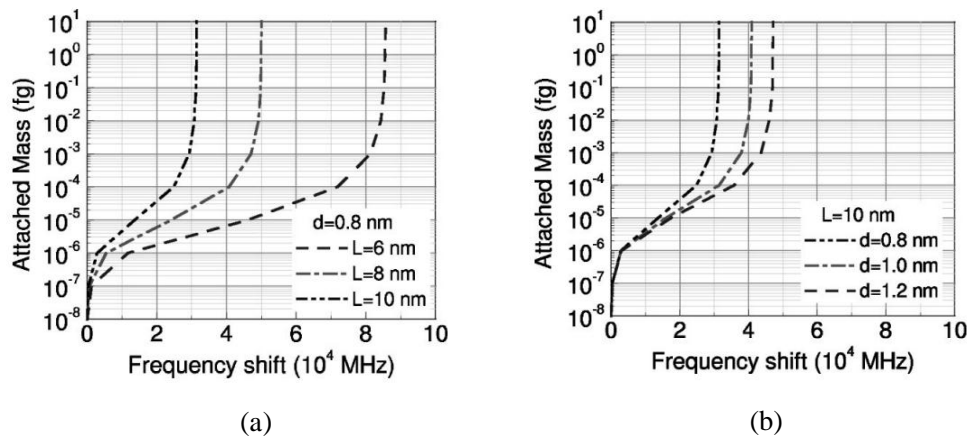

(a)   (b)

Figure 6. Resonant frequency shifts of cantilevered nanotubes with different lengths (**a**) and tube diameter (**b**) vs. attached mass. Adapted with permission from [37], Copyright AIP Publishing LLC, 2004.

Since DWCNTs have higher stiffness and strength, thermal and chemical stability than single-walled CNTs, the potential of DWCNTs as a nano mass sensor was also explored [38–40]. The inner and outer walls of the DWCNT were modelled as finite elements [38] or elastic beams [39,40], and the interaction force between the two walls was considered as a spring element connecting the two layers by van der Waals (vdW) interaction. The interlayer interaction is described by the vdW potential. The most common expression of Lennard–Jones potential is utilized to express the interaction of carbon atoms located on the two walls, given by

$$U(R) = 4\varepsilon\left[\left(\frac{\rho}{R}\right)^{12} - \left(\frac{\rho}{R}\right)^6\right], \tag{3}$$

where R is the inter atomic distance, ε is the depth of the potential, and σ is the finite distance at which the interatomic potential is zero. The pressure caused by the vdW interaction can be described by

$$p = c(u_2 - u_1), \tag{4}$$

where u_1 and u_2 are the vibrational deflection of inner and outer walls of DWCNTs, respectively. c is the vdW interaction coefficient between the walls. The vdW interaction coefficients can be estimated using Equation (5) [41]

$$c = \frac{320 \times (2R_j)\,\text{erg/cm}^2}{0.16\Delta^2}, \qquad \Delta = 0.142\,\text{nm}, \tag{5}$$

where R_j is the center line radius of the jth nanotube, and Δ is the length of carbon–carbon (C–C) bond.

　　In the finite element model (FEM) [38], the element equation constructed by the global stiffness and mass matrices can be assembled. The governing coupled equations for the displacement are given by

$$K_1 u_1 + M_1 \ddot{u}_1 = c(u_2 - u_1), \tag{6}$$

$$K_2 u_2 + M_2 \ddot{u}_2 = c(u_1 - u_2), \tag{7}$$

where K_1, K_2 are stiffness matrices, M_1, M_2 are mass matrices, and the wall deflections of DWCNT are given as

$$u_j = Y_j e^{i\omega t}, \tag{8}$$

and Y_j, $j = 1, 2$, are the vibrational amplitudes and ω is the vibrational frequency.

　　According to Equations (6)–(8), the element equation for global system can be written as

$$\begin{bmatrix} K_1 + c & -c \\ -c & K_2 + c \end{bmatrix} \begin{Bmatrix} Y_1 \\ Y_2 \end{Bmatrix} - \omega^2 \begin{bmatrix} M_1 & 0 \\ 0 & M_2 \end{bmatrix} \begin{Bmatrix} Y_1 \\ Y_2 \end{Bmatrix} = 0. \tag{9}$$

　　The vibrational frequency of DWCNTs can be obtained by a nontrivial solution of Equation (9).

　　For the continuum mechanics, Patel and Joshi [39] derived a second order governing differential equation of Euler beam model and considered nonlinear vdW interaction between nanotubes, by using a single-mode Galerkin approximation. The dynamic response of the DWCNT-based mass sensor was analyzed based on time response, Poincaré maps, and fast Fourier transformation. The results showed that the appearance of regions of periodic, subharmonic and chaotic behavior were strongly dependent on mass, inner and outer nanotubes and the geometric imperfections of DWCNTs. Shen et al. [40] analyzed the vibration frequency of DWCNT-based mass sensor using nonlocal Timoshenko beam theory. The natural frequencies of a nonlocal cantilever beam attached to a tip mass were computed using the transfer function method. They assumed that the inner and outer walls of DWCNTs had different lengths, and the atom-resolution mass was attached to the free end of the inner nanotube. Effects of the attached mass and outer-to-inner tube length ratio on the natural frequencies were discussed. The results showed that the mass sensor based on DWCNTs with different wall lengths had a noticeable advantage over that based on SWCNTs. The mass sensitivity of DWCNT-based sensor could be enhanced when short DWCNTs were used, especially for larger attached mass. The nonlocal Timoshenko beam model was more adequate than the nonlocal Euler–Bernoulli beam model for short DWCNT sensors. The mass sensing characteristics of DWCNT based nanobalances can reach up to 0.1 Zeptograms [37].

　　It is obvious that mass sensitivity of nano-mass detection system can be improved by using smaller sized CNTs since CNT-based resonator results high oscillation frequency. In order to increase sensitivity of the resonators, the author Natsuki and co-workers proposed using a double end fixed CNT with applied tensile loads and investigated the possibility of application [42,43]. Figure 7 shows a schematic diagram of the clamped CNT beam, subjected to an axial force and carrying an attached concentrated mass m_c. Based on the continuum model with the Euler–Bernoulli beam, the motion equations of a freely vibrating CNT under the axial tensile load N can be given as [42]
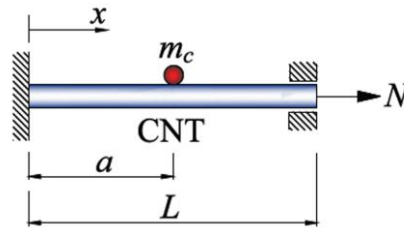
Figure 7. Schematic diagram of clamped carbon nanotube (CNT) beam model with attached mass under tensile load.

$$\frac{\partial^4 Y_1(x,t)}{\partial x^4} - \frac{N}{EI}\frac{\partial^2 Y_1(x,t)}{\partial x^2} - \frac{\rho A \omega^2}{EI}\frac{\partial^2 Y_1(x,t)}{\partial t^2} = 0 \qquad 0 \le x \le a, \tag{10}$$

$$\frac{\partial^4 Y_2(x,t)}{\partial x^4} - \frac{N}{EI}\frac{\partial^2 Y_2(x,t)}{\partial x^2} - \frac{\rho A \omega^2}{EI}\frac{\partial^2 Y_2(x,t)}{\partial t^2} = 0 \qquad a \le x \le L, \tag{11}$$

where Y_j ($j = 1, 2$) are the vibration amplitudes of the flexural deflection, ω is the circular frequency, EI is the flexural stiffness of CNT, A is the cross-sectional area, ρ is the mass density, L is the length of CNT, a is the position in which concentrated mass is attached, x is the axial coordinate and t is the time.

According to corresponding boundary conditions such as bound states and continuum states, the resonant frequency (ω) of the CNT resonators with an attached concentrated mass can be derived from Equations (10) and (11), and given by the following matrix equation:

$$|M(m_c, \omega)|_{8 \times 8} = 0. \tag{12}$$

Based on Rayleigh's energy method [42], the differential equation of CNT bending moment can be given by

$$y(x) = A\cosh(\alpha x) + B\sinh(\alpha x) + \frac{Px}{2N} + \frac{M_0}{N}, \tag{13}$$

where P is mass load acted on the middle of the CNT, and M_0 is the moment at the left clamped end. The moment M_0, the integration constants of A and B, can be determined from the clamped boundary conditions:

$$y(0) = y'(0) = y'(L/2) = 0. \tag{14}$$

Moreover, the maximum kinetic energy of the CNT beam can accordingly be given by

$$T_{\max} = \frac{1}{2}\int_0^{L/2} \frac{2m_{CNT}}{L}\{\dot{y}(x)\}^2 dx, \tag{15}$$

where m_{CNT} ($m_{CNT} = \rho AL$) is the mass of the CNT resonator.

Substituting Equation (13) into Equation (15) and according to the relationship between force and deflection, the equivalent stiffness of CNT beam can be obtained

$$k_{eq} = \frac{P}{y_{\max}} = \frac{2N\alpha}{2\tanh\frac{\alpha L}{4}\sinh^2\frac{\alpha L}{4} + \left(\frac{\alpha L}{2} - \sinh\frac{\alpha L}{2}\right)} \tag{16}$$

and $\alpha = \sqrt{\frac{N}{EI}}$.

Thus, the resonant frequency of the CNT resonators carrying concentrated mass (m_c) yields

$$\omega = \frac{1}{2\pi}\sqrt{\frac{k_{eq}}{\phi \rho AL + m_c}}, \tag{17}$$

where

$$\phi = \frac{3\beta^2}{2} - \frac{\alpha\beta\gamma L}{2} + \frac{\alpha^2\gamma^2 L^2}{12} + \left(2\beta\gamma + \frac{4\gamma^2 - 4\beta^2}{\alpha L}\right)\sinh\frac{\alpha L}{2}$$
$$- 2\gamma^2\cosh\frac{\alpha L}{2} + \frac{\beta^2 + \gamma^2}{2\alpha L}\sinh\alpha l - \frac{2\beta\gamma}{\alpha L}\sinh^2\frac{\alpha L}{2} - \frac{\gamma^2}{2} \tag{18}$$

and

$$\beta = \frac{\tanh\frac{\alpha l}{4}}{2\tanh\frac{\alpha L}{4}\sinh^2\frac{\alpha L}{4} + \left(\frac{\alpha L}{2} - \sinh\frac{\alpha L}{2}\right)}, \gamma = \frac{1}{2\tanh\frac{\alpha L}{4}\sinh^2\frac{\alpha L}{4} + \left(\frac{\alpha L}{2} - \sinh\frac{\alpha L}{2}\right)}. \tag{19}$$

Figure 8 shows a comparison of the resonant frequency between the Euler–Bernoulli beam model and the Rayleigh's energy method as a function of attached mass. The result obtained using Rayleigh's energy method was a little higher than that obtained by the continuum elastic method when the mass of the sensor was less than 10^{-3} zg (the error range being within 2.4%). It was observed that the two results were very consistent with each other for increasing attached mass. The error range was within only 0.06% when the attached mass reached to 10^{-1} zg. The two analytical models were proven to be successful and effective owing to a good agreement between them.

Based on the Euler–Bernoulli beam model, Figure 9 shows the resonant frequency shifts vs. attached concentrated mass for the CNT beam with axial force and without axial force. The results show that the frequency shift of the CNT resonator was increased by axial tensile loads, and the difference in the frequency shifts increased with the increase of attached mass. The high tensile strength of CNT (up to 63 GP [44]) suggested that higher mass sensitivity could be obtained by increasing tensile force acting on the CNTs. The frequency shift of the CNT resonator for an attached mass larger than 10^{-1} zg was found to increase up to 28% when an axial tensile load of 20 nN, corresponding to the tensile stress of about 19 GPa, was applied on the CNTs. The results showed that the sensitivity of CNT-based sensor under the tensile load can reach at least 10^{-1} zg, which demonstrates higher accuracy than the 1 zg sensitivity reported by Li and Chou [37].
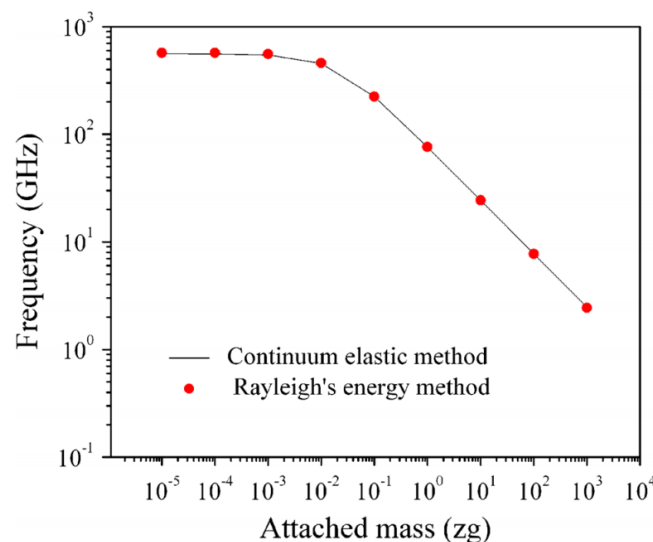

Figure 8. Comparison of the resonant frequency between the Euler–Bernoulli beam model and the Raleigh's energy method. Adapted with permission from [42], Copyright Springer, 2014.

Furthermore, in Ref. [43], Natsuki et al. proposed using the nonlocal Euler–Bernoulli beam model for investigating the resonant frequency of CNT resonators. The nonlocal elasticity theory was developed to incorporate the size effect by introducing an intrinsic length scale, which gave the information about the forces between atoms. Nonlocal beam theory has been widely used to study the vibration properties of CNTs and has been proven to be more effective than other theoretical approaches such as the Euler beam model. In the case of nanostructures, the nonlocal effects considered

in the nonlocal elasticity theory played an important role in the vibration analysis and determined by the magnitude of nonlocal parameters [45].

For the theoretical approach considering nonlocal parameter $e_0 a / L$ (e_0 is material constant, a the internal characteristic length and L is the external characteristic length), the resonant frequency of the CNT resonators based on Rayleigh's energy method can be obtained as the following:

$$\omega = \frac{1}{2\pi} \sqrt{\frac{k_{eq}}{(\phi + \mu)\rho AL + m_c}},\qquad(20)$$

where k_{eq} is defined as Equation (16), and ϕ defined as Equation (18). The parameter μ is given by

$$\mu = \left(\frac{\frac{\alpha(\beta^2+\gamma^2)L}{2}\sinh\alpha L - \cosh\alpha L + 4\alpha\beta\gamma L \cosh\frac{\alpha L}{2}}{-4\alpha\gamma^2 L\sinh\frac{\alpha L}{2} + \frac{3\alpha^2 L^2(\gamma^2-\beta^2)}{2} - 3\alpha\beta\gamma L} \right) \left(\frac{e_0 a}{L}\right)^2. \qquad(21)$$

Figure 10 shows the variation of the resonant frequency of the clamped CNT with the attached mass. The influence of the nonlocal parameter $e_0 a / L$ on the frequency shift was investigated, showing increase with increasing attached mass, especially for larger than 1.0 zg. The mass sensitivity of CNT resonator usually depends on the variation of the frequency shift with attached mass. Therefore, the results indicated that the nanomass in the order of 0.001–1.0 zg had higher sensitivity to the CNT resonator.
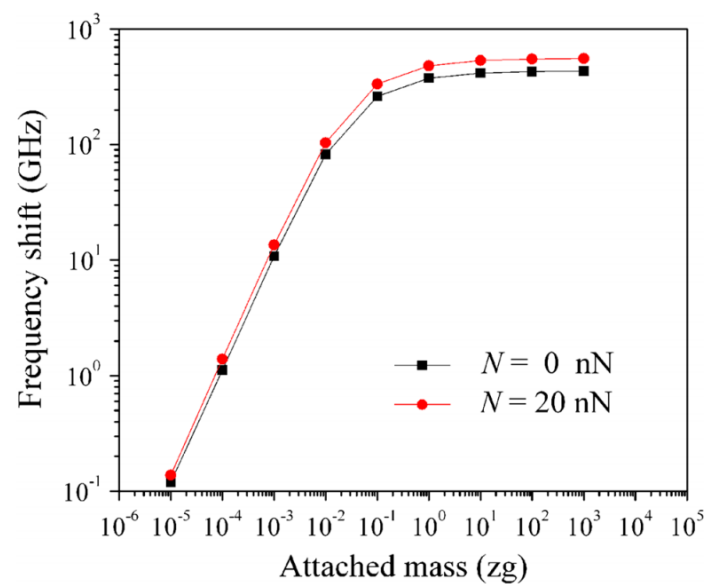

Figure 9. Resonant frequency shifts vs. attached concentrated mass for the CNT beam with axial force and without axial force. Adapted with permission from [42], Copyright Springer, 2014.
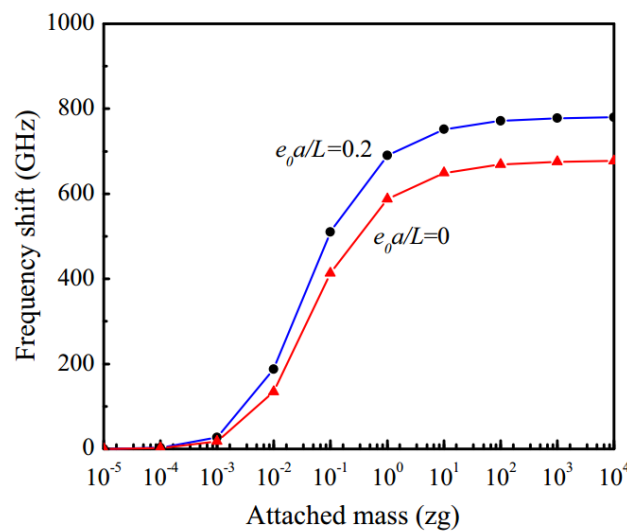
Figure 10. Effect of the nonlocal coefficient on the resonant frequency of the CNTs under attached different nanomasses. Adapted with permission from [43], Copyright Springer, 2015.

3. CNT Probes for Atomic Force Microscope

3.1. Fabrication and Structures of CNT Tip

Atomic Force Microscope (AFM) was a very useful instrument for imaging, measuring and characterizing nanoscale features [46]. However, the poorly characterized silicon and nitride probe tips currently employed in AFM limit some applications since conventional silicon tips can easily break during an impact on the scanned surface. CNTs are potentially ideal materials for AFM probe application due to their robust mechanical properties and well-defined geometry such as a small diameter and high aspect ratio [47–49]. There were some reports on the use of CNT probes tip increase the sensitivity and the resolution in the AFM. The research group of Prof. Dai first attached individual CNTs with several micrometers to the silicon microcantilever sensing tips of an AFM [50]. They demonstrated that the CNT tips were resistant to damage from tip crashes because of their flexibility and stiffness. Figure 11 shows the SEM image of a CNT scanning probe (a), and a schematic showing the ability of the CNT tip to trace the profile of trenches with deep and narrow features (b). Due to the large aspect ratio of CNT, AFM, coupled with a high-aspect-ratio CNT scanning probe, exhibited the ability to resolve features. Their exceptional mechanical strength and the ability to buckle reversibly enabled the resolution of steep and deep nanoscale features.
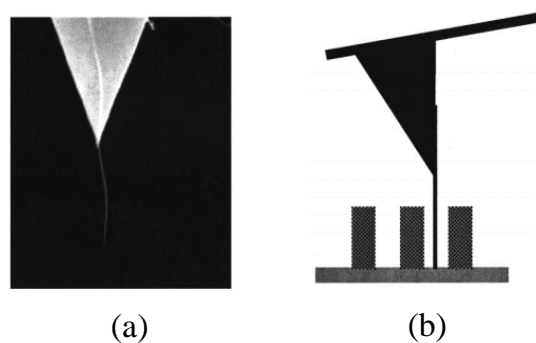

(a)   (b)

Figure 11. SEM image of a multi-walled CNT (MWCNT) tip and schematic of the CNT tip to trace the profile of trenches. (**a**) SEM image of a CNT scanning probe, (**b**) the ability of the CNT tip to trace the profile of trenches with deep and narrow features. Adapted with permission from [51], Copyright AIP Publishing LLC, 2002.

The investigation and development of CNT AFM probes includes the fabrication process of CNT probes and their mechanical stability in structures. CNT probes can be provided by manual attachment of a CNT to the tip of the AFM cantilever or by growing a CNT from the ends of the silicon tip of the AFM probe based on chemical vapor deposition (CVD) process. The welding method was developed for fixing CNT to the silicon probe end [52,53]. CVD methods reported by Prof. Hafner et al. [54,55] allowed aligned growth of CNTs on the silicon probe surface, and the diameter and length of CNT could be controlled by adjusting the growth time and its growth temperatures (Figure 12) [56]. Hafner et al. successfully fabricated CNT AFM tips using ethylene and iron catalysis deposited on commercial silicon-cantilever-tip assemblies. Individual CNTs grew from the pores etched in the flattened area at the tip after reaction of the electrodeposited iron catalytic tips with ethylene at elevated temperature. SEM images demonstrated that these nanotube tips grew in an ideal orientation for AFM imaging (see Figure 12a). Cumings and Zettl [57] fabricated and demonstrated the controlled and reversible telescopic extension of CNTs. Figure 13 shows TEM images of a telescoped nanotube, which has nine shells and a four-shell core was extracted upon telescoping. Their results suggested that MWCNTs had great promise for the nanomechanical or NEMS applications. The preparation of DWCNTs with a short outer wall could be carried out by the method of burning the outer wall using an electric current [58]. Compared to SWCNTs, DWCNTs or MWCNT with a protruding inner tube as AFM probes would be better due to the high spatial resolution. Using DWCNT, with a shorter outer wall, the CNT probes were expected to have high resolution and high stability due to thick-walled structures and small probe tips.

The resolution of AFM is mainly determined by the probe's shape and mechanical properties, especially the dimension of the probe end tip. A fundamental issue of the application for CNTs as AFM probes is to how design and obtain the buckling stability of CNTs with a small tip diameter. By now, there are several methods to investigate the instability properties of CNTs when subjected to an axial force. The instability phenomenon of CNTs under compressive loading was observed experimentally by TEM [59–62]. Figure 14 shows the direct observation of nanotube buckling characterization by in situ transmission TEM. The TEM images of Figure 14a–f clarified a series of deformation processes for CNTs under compression force.
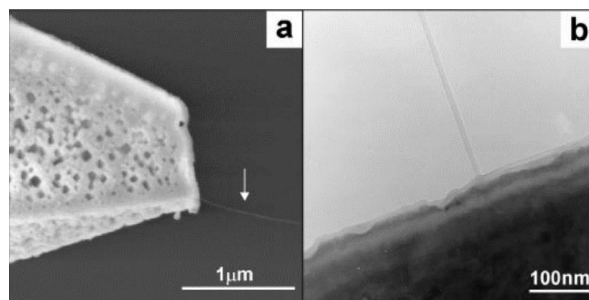

Figure 12. Electron microscopy of chemical vapor deposition (CVD) nanotube tips. (**a**) SEM image of an MWCNT grown from a silicon-cantilever-tip assemblies; (**b**) TEM image of the CNT tip. Adapted with permission from [55], Copyright PNAS, 2000.
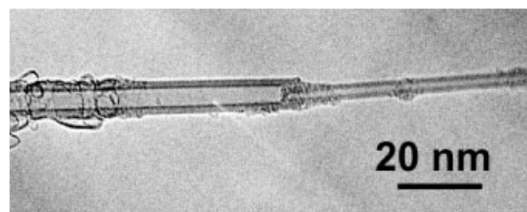

Figure 13. TEM image of a telescoped nanotube. Adapted with permission from [57], Copyright AAAS, 2000.

However, the dynamics experiments of nanotube buckling remains a major challenge because of the nanometric scale of CNTs. Until now, the experimental investigation is very difficult to accurately measure the buckling load. Thus, the theoretical study is mainly used for predicting the buckling loads and buckling modes of CNT structures.
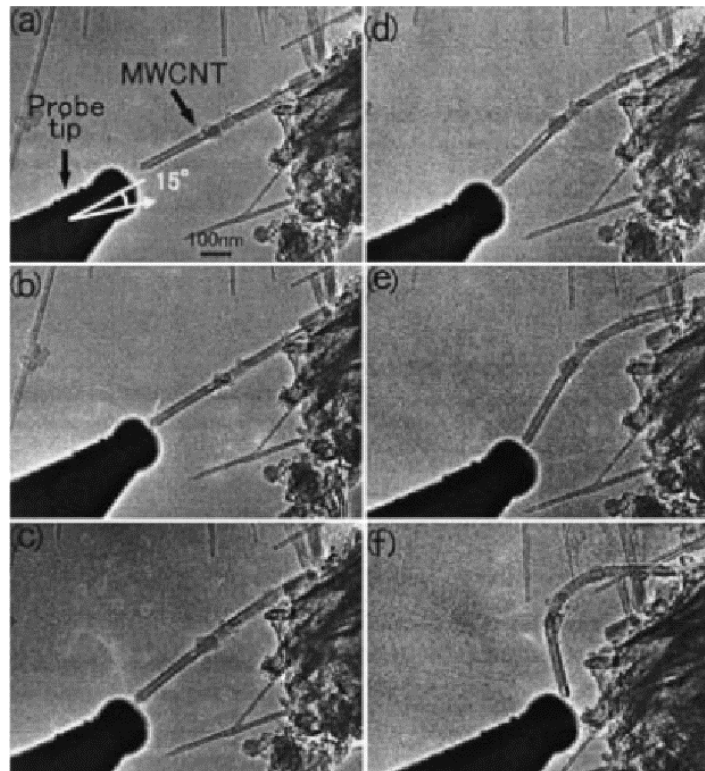

Figure 14. Series of TEM images of deformation processes for MWNTs initiated by applying compressive force in the sample direction. Adapted with permission from [62], Copyright MDPI, 2012.

3.2. Theoretical Mode and Approach of Buckling Properties

Under axial compression, CNTs are not so strong compared with tension loads due to the high aspect ratio. Therefore, the buckling property of CNTs is very important in order to understand the strength and failure of CNTs used as CNT probes of AFM. To investigate buckling behavior of the CNTs, some theoretical research of buckling analysis, such as compression buckling [63–65], torsional buckling [66], bending buckling [67], and radial buckling [68], has been carried out in the last decade. The first detailed analysis on the buckling of SWCNTs under axial compression was reported by Yakobson et al. [69] based on both MD method and continuum shell model. They found that CNTs could be reversibly switched into different morphological patterns when subjected to large deformations. As shown in Figure 15, the buckling phenomenon of CNT subjected to axial compression was simulated. Figure 15a displays four singularities corresponding to shape changes of the CNT with a length of 6 nm and diameter of 1 nm. The presence of four singularities at higher strains was quite a striking feature, and the patterns shown in Figure 15b–e illustrate the corresponding morphological changes. The results showed that CNTs were remarkably resilient, sustaining extreme strain without brittleness, plasticity, or atomic rearrangement. They also indicated that the peculiar behavior beyond Hooke's law could be well described by a continuum shell model. Comparing the results obtained by continuum shell model with those from MD simulations, Yakobson et al. found that the results were in good agreement with one another.
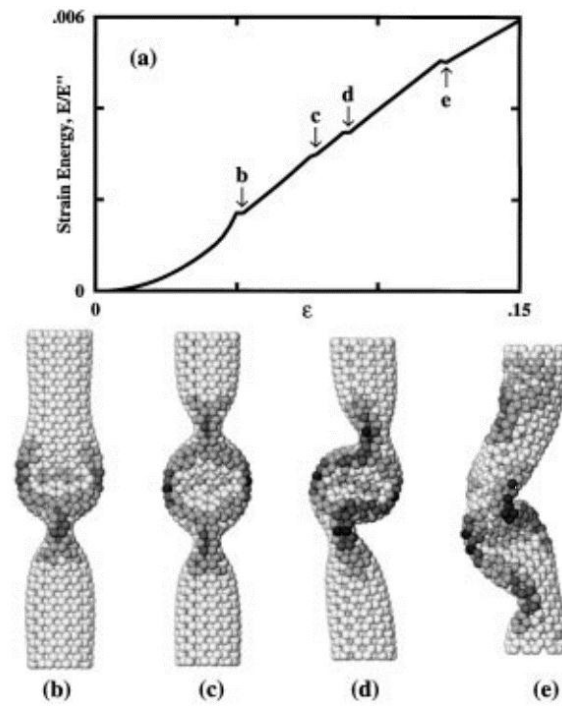
Figure 15. Series of TEM images of deformation processes for MWNTs initiated by applying compressive force in the sample direction. Adapted with permission from [69], Copyright American Physical Society, 1996.

The Donnell shell models (DSM) has been widely used to evaluate the buckling properties of CNTs under compression, bending and torsion. Silvestre [70] presented a study on the buckling behaviors of SWCNTs under torsion by using DSM. Straightforward analytical expressions to calculate the critical angle of twist for CNTs were derived. Despite its simplicity, the procedure presented was shown to give accurate simulation results for a wide range of CNT length and diameter. Hu et al. [71] investigated the effects of CNT microstructure on the wave propagation of both SWCNTs and DWCNTs, based on a nonlocal shell model. The nonlocal elastic shell theory was showed to provide better results for the wave dispersion than the classical shell theory. There is good agreement between the elastic shell theory and the MD method. The nonlocal parameters could be suggested by MD-based estimation.

Based on the successful application of the cylindrical shell model for SWCNT [69], the multiple-shell model [70–74] and the beam model [75,76] were proposed and developed for simulating buckling properties of MWCNTs under axial compression. The adjacent nanotubes for MWCNTs were coupled to each other by the vdW interaction. The vdW interaction force $p_{k(k+1)}$ between tube k and $k + 1$ of an N-walled CNT ($k = 1, 2, \cdots, N - 1$) is proportional to the radial deflection ($w_{k+1} - w_k$) between the two neighboring nanotubes, given as

$$p_{k(k+1)} = c_{k(k+1)} \cdot (w_{k+1} - w_k), \tag{22}$$

where the vdW interaction coefficient is given by [74]

$$c_{k(k+1)} = \frac{\pi \varepsilon R_k R_{k+1} \sigma^6}{\Delta^4} \left[\frac{1001 \sigma^6}{3} H_{k(k+1)}^7 - \frac{1120}{9} H_{k(k+1)}^{13} \right] \tag{23}$$

and

$$H_{k(k+1)}^m = (R_k + R_{k+1})^{-m} \int_0^{\pi/2} \frac{d\theta}{\left(1 - K_{k(k+1)} \cos^2 \theta\right)^{m/2}} \ (m = 7, 13), \ K_{k(k+1)} = \frac{4 R_k R_{k+1}}{(R_k + R_{k+1})^2}, \tag{24}$$

where Δ is the carbon–carbon bond length, and R_k is the radius of nanotube k, σ and ε are the vdW radius and the well depth of the Lennard–Jones potential, respectively.

Based on continuum models, the author Natsuki and co-investigators proposed DWCNT tips with shorter outer wall [77]. The CNT structures are able to increase the stability of AFM nanoprobes and to obtain higher resolution due to small tip diameter. This makes the buckling investigation of DWCNTs with different wall lengths more significant from both theoretical and practical perspectives. Figure 16 shows an analytical model of cantilevered DWCNTs with different inner and outer nanotube lengths, and L_2 and L_1 are the inner and outer lengths, respectively.
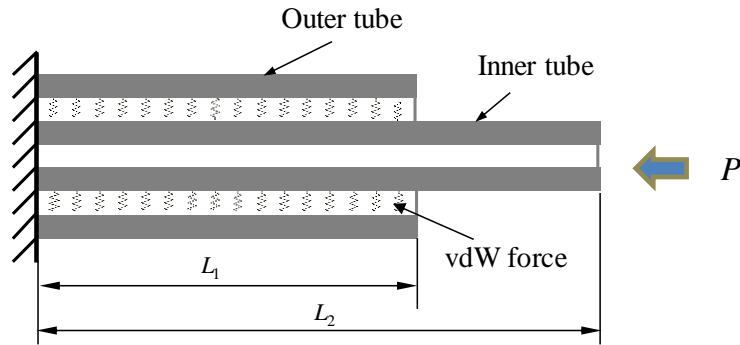

Figure 16. Schematic diagram of clamped CNT with different tube length.

As shown in Figure 16, the governing differential equations of the inner and outer nanotubes, in which adjacent walls are coupled to each other by the vdW interaction forces, can be given by

$$(EI)_1 \frac{d^4 w_1}{dx^4} + P \frac{d^2 w_1}{dx^2} = c_{12} \cdot (w_2 - w_1) \ 0 \leq x \leq L_1, \tag{25}$$

$$(EI)_2 \frac{d^4 w_2}{dx^4} = c_{21} \cdot (w_1 - w_2) \ 0 \leq x \leq L_1, \tag{26}$$

$$(EI)_3 \frac{d^4 w_3}{dx^3} + P \frac{d^2 w_3}{dx^2} = 0 \ L_1 \leq x \leq L_2, \tag{27}$$

where $w_j (j = 1, 2)$ are the transverse deflections of the inner and outer nanotubes, respectively, w_3 is the transverse deflection of the inner nanotube between L_1 and L_2, and $(EI)_j$ $(j = 1, 2, 3)$ is the flexural stiffness of the nanotubes.

In order to obtain the solution of Equations (25)–(26), the corresponding boundary conditions, considering a cantilevered DWCNT subjected to an axial loading P, are given as follows:

(a)   For the inner and outer nanotubes with fixed ends:

$$w_1(0) = \left. \frac{dw_1(x)}{dx} \right|_{x=0} = w_2(0) = \left. \frac{dw_2(x)}{dx} \right|_{x=0} = 0; \tag{28}$$

(b)   For the inner and outer nanotubes with free ends:

$$\left. \frac{d^2 w_2(x)}{dx^2} \right|_{x=L_1} = \left. \frac{d^3 w_2(x)}{dx^3} \right|_{x=L_1} = \left. \frac{d^2 w_3(x)}{dx^2} \right|_{x=L_2} = 0, \ (EI)_3 \left. \frac{d^3 w_3(x)}{dx^3} \right|_{x=L_2} + P \left. \frac{dw_3(x)}{dx} \right|_{x=L_2} = 0; \tag{29}$$

(c)   For the continuous conditions at position L_1, the relationships of displacement and force between the transverse deflections w_1 and w_3 are given as:

$$w_1(L_1) = w_3(L_1), \ \frac{dw_1(x)}{dx}\Big|_{x=L_1} = \frac{dw_3(x)}{dx}\Big|_{x=L_1}, \ \frac{d^2w_1(x)}{dx^2}\Big|_{x=L_1} = \frac{d^2w_3(x)}{dx^2}\Big|_{x=L_1},$$
$$(EI)_1 \frac{d^3w_1(x)}{dx^3}\Big|_{x=L_1} + P\frac{dw_1(x)}{dx}\Big|_{x=L_1} = (EI)_3 \frac{d^3w_3(x)}{dx^3}\Big|_{x=L_1} + P\frac{dw_3(x)}{dx}\Big|_{x=L_1}. \tag{30}$$

Substituting the deflection functions of the inner and outer nanotubes, w_1, w_2 and w_3, into the above boundary conditions, the buckling load P_c can be obtained from eigenvalue analysis.

As shown in Figure 17, the buckling instability of CNTs can occur in different mode shapes based on the proposed theoretical model. The fundamental mode 1, among three modes, has the maximum instability, whose critical buckling strain was 0.0051. The buckling strains of CNTs with the mode 2 and 3 were 0.024 and 0.07, respectively. Although the only inner nanotube was subjected to an axial load, the deflection of the outer nanotube happens similar to that of the inner nanotubes through the vdW interaction force between adjacent nanotubes. Figure 18 shows the buckling stress of the DWCNT as a function of length ratio L_{Outer}/L_{Inner} for the fundamental mode, associated with the lowest buckling load. In the Figure 18, the curve (A) stands for the fixed inner tube and variable outer tube, and the curve (B) for the fixed outer tube and variable inner tube. The influences of structural parameter of the length aspect on the buckling stress of DWCNT AFM probes were significant based on the length mismatch between inner and outer nanotubes. It was found that the DWCNT AFM probe with type (A) showed increasing buckling stability as the outer nanotube elongates. The buckling stress of the CNT probe was about three times larger than the curve (B), where the SWCNT or the inner nanotube was fixed. Due to the reinforcement effect of the outer nanotube, it was possible to obtain better stability when using the CNT structure covered with the outer layer for the probe.
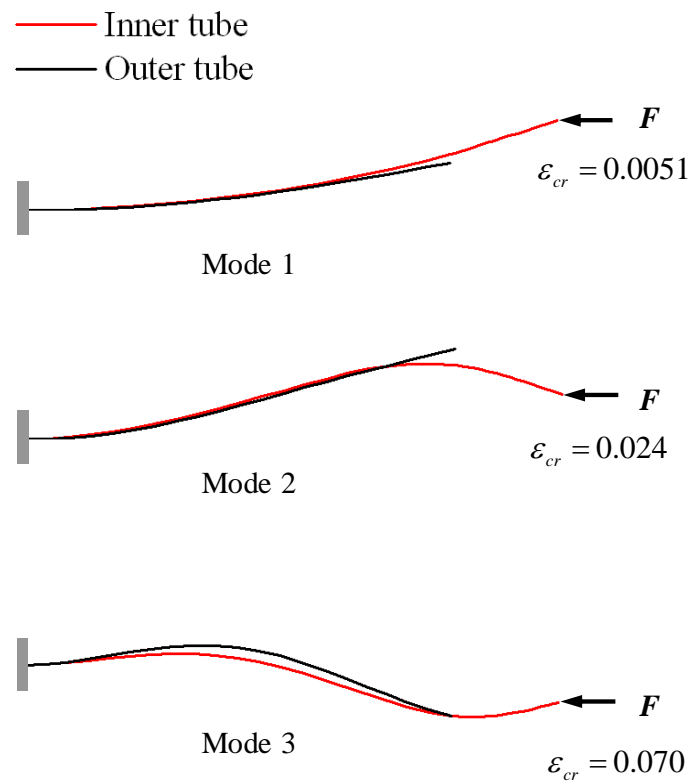

Figure 17. Schematic diagram describing the buckling instability of cantilevered $(16,0)@(26,0)$ DWCNTs, with the inner tube of 20 nm and the length ratio of outer to inner tubes of 20. Adapted with permission from [77], Copyright Elsevier, 2011.
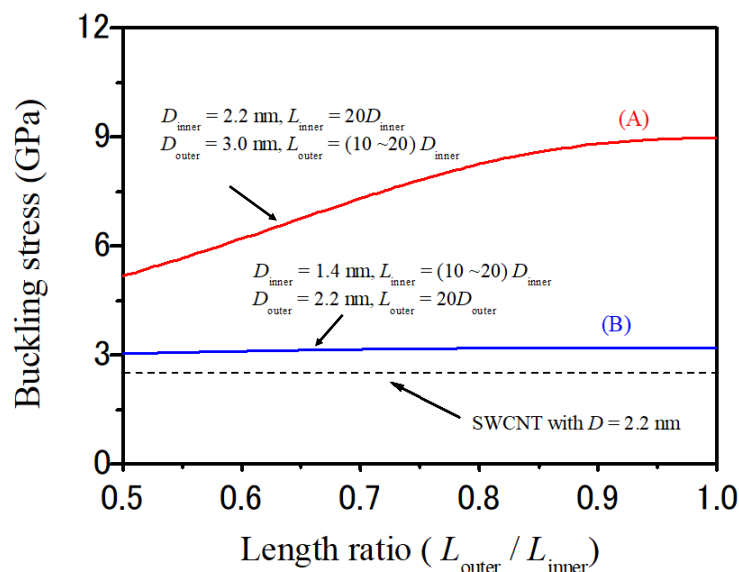
Figure 18. Variation of the buckling stress of DWCNTs with the length ratio for the first bending mode 1. Adapted with permission from [77], Copyright Elsevier, 2011.

4. Conclusions

The discovery of CNTs in the early 1990s has stimulated ever-broader science and engineering devoted to production and application of various CNTs. Due to their special structures, exceptional mechanical and physical properties, CNTs hold many potential applications in the nanotechnology industry. Among the mechanical behaviors, the vibration and buckling instability have a significant impact on the performance of CNT-based nanosensor or nanodevices. Thus, it is crucial for us to understand the mechanical behaviors of the unique CNTs. The review discusses the application of CNTs used as nanomechanical sensors, and their performance predicted by theoretical model and analysis. Actually, the technology and experimental work on CNT-based sensor is still in its infancy stage. Owing to a lack of an efficient or accurate characterization technique, a quantitative experimental study is not feasible for controlling extremely small size of CNTs. With the development of CNT materials with specific structures and the micro processing technology [78,79], it is expected that high-performance of CNT-based sensors and nanodevices will be realized in the near future.

Conflicts of Interest: The author declares no conflict of interest.

References

1. Iijima, S. Helical microtubules of graphitic carbon. *Nature* **1991**, *354*, 56–58. [CrossRef]
2. Bandaru, P.R. Electrical properties and applications of carbon nanotube structures. *J. Nanosci. Nanotechnol.* **2007**, *7*, 1–29. [CrossRef]
3. Abdalla, S.; Al-Marzouki, F.; Al-Ghamdi, A.A.; Abdel-Daiem, A. Different technical applications of carbon nanotubes. *Nanoscale Res. Lett.* **2015**, *10*, 358. [CrossRef] [PubMed]
4. Thostensona, E.T.; Renb, Z.; Choua, T.W. Advances in the science and technology of carbon nanotubes and their composites: A review. *Compos. Sci. Technol.* **2001**, *61*, 1899–1912. [CrossRef]
5. Popov, V.N. Carbon nanotubes: Properties and application. *Mater. Sci. Eng.* **2004**, *43*, 61–102. [CrossRef]
6. Paradise, M.; Goswami, T. Carbon nanotubes-Production and industrial applications. *Mater. Des.* **2007**, *28*, 1477–1489. [CrossRef]
7. Qian, D.; Wagner, G.J.; Liu, W.K.; Yu, M.F.; Ruoff, R.S. Mechanics of carbon nanotubes. *Appl. Mech. Rev.* **2002**, *55*, 495–533. [CrossRef]
8. Natsuki, T.; Endo, M. Structural dependence of nonlinear elastic properties for carbon nanotubes using a continuum analysis. *Appl. Phys. A* **2005**, *80*, 1463–1468. [CrossRef]

9. Yu, M.F.; Lourie, O.; Dyer, M.J.; Moloni, K.; Kelly, T.F.; Ruoff, R.S. Strength and breaking mechanism of multiwalled carbon nanotubes under tensile load. *Science* **2000**, *287*, 637–640. [CrossRef] [PubMed]

10. Wei, B.Q.; Vajtai, R.; Ajayan, P.M. Reliability and current carrying capacity of carbon nanotubes. *Appl. Phys. Lett.* **2001**, *79*, 1172–1174. [CrossRef]

11. Alemán, B.J.; Sussman, A.; Mickelson, W.; Zettl, V. A carbon nanotube-based NEMS parametric amplifier for enhanced radio wave detection and electronic signal amplification. *J. Phys. Conf. Ser.* **2011**, *302*, 1–6. [CrossRef]

12. Rajoria, H.; Jalili, N. Passive vibration dampingenhancement using carbon nanotube-epoxy reinforced composites. *Comps. Sci. Technol.* **2005**, *65*, 2079–2093. [CrossRef]

13. Rotkin, S.V. Nanotube MEMS: Modeling extreme nanoscale devices. *Proc. SPIE* **2009**, *7318*, 1–13.

14. Baughman, R.H.; Zakhidov, A.A.; de Heer, W.A. Carbon nanotubes—The route toward applications. *Science* **2002**, *297*, 787–792. [CrossRef] [PubMed]

15. Zang, X.; Zhou, Q.; Chang, J.; Liu, Y.; Liwei, L. Graphene and carbon nanotube (CNT) in MEMS/NEMS applications. *Microelectron. Eng.* **2015**, *25*, 192–206. [CrossRef]

16. Yan, Y.; Miao, J.; Yang, Z.; Xiao, F.X.; Yang, H.B.; Liu, B.; Yang, Y. Carbon nanotube catalysts: Recent advances in synthesis, characterization and applications. *Chem. Soc. Rev.* **2015**, *44*, 3295–3346. [CrossRef] [PubMed]

17. Rafique, M.M.A.; Iqbal, J. Production of carbon nanotubes by different routes- A review. *J. Encapsul. Adsorpt. Sci. (JEAS)* **2011**, *1*, 29–34. [CrossRef]

18. Sazonova, V.; Yaish, Y.; Üstünel, H.; Roundy, D.; Arias, T.A.; McEuen, P.L. A tunable carbon nanotube electromechanical oscillator. *Lett. Nat.* **2004**, *431*, 284–287. [CrossRef] [PubMed]

19. Che, Y.; Chen, H.; Gui, H.; Liu, J.; Liu, B.; Zhou, C. Review of carbon nanotube nanoelectronics and microelectronics. *Semicond. Sci. Technol.* **2014**, *29*, 073001. [CrossRef]

20. Hall, A.R.; An, L.; Liu, J.; Vicci, L.; Falvo, M.R.; Superfine, R.; Washburn, S. Experimental measurement of single-wall carbon nanotube torsional properties. *Phys. Rev. Lett.* **2006**, *96*, 256102. [CrossRef] [PubMed]

21. Knobel, R.G. Mass sensors: Weighing single atoms with a nanotube. *Nat. Nanotechnol.* **2008**, *3*, 525–526. [CrossRef] [PubMed]

22. Cao, Q.; Rogers, J.A. Random networks and aligned arrays of single-walled carbon nanotubes for electronic device applications. *Nano Res.* **2008**, *1*, 259–272. [CrossRef]

23. Kauth, C.; Pastre, M.; Kayal, M. A novel approach to high-speed high-resolution on-chip mass sensing. *Microelectron. J.* **2014**, *45*, 1648–1655. [CrossRef]

24. Yang, Y.T.; Callegari, C.; Feng, X.L.; Ekinci, K.L.; Roukes, M.L. Zeptogram-scale nano-mechanical mass sensing. *Nano Lett.* **2006**, *6*, 583–586. [CrossRef] [PubMed]

25. Tretkoff, E. Weighing device achieves zeptogram-level sensitivity. *APS News* **2005**, *14*, 5.

26. Poncharal, P.; Wang, Z.L.; Ugarte, D.; de Heer, W.A. Electrostatic defections and electromechanical resonances of carbon nanotubes. *Science* **1999**, *283*, 1513–1516. [CrossRef] [PubMed]

27. Wang, Z.L.; Poncharal, W.A.; de Heer, W.A. Measuring physical and mechanical properties of individual carbon nanotubes by in situ TEM. *J. Phys. Chem. Solids* **2000**, *61*, 1025–1030. [CrossRef]

28. Jensen, K.; Kim, K.; Zettl, A. An atomic-resolution nanomechanical mass sensor. *Nat. Nanotechnol.* **2008**, *3*, 533–537. [CrossRef] [PubMed]

29. Li, J.J.; Zhu, K.D. Weighing a single atom using a coupled plasmon–carbon nanotube system. *Sci. Technol. Adv. Mater.* **2012**, *13*, 1–6. [CrossRef] [PubMed]

30. Kühn, S.; Håkanson, U.; Rogobete, L.; Sandoghdar, V. Enhancement of single-molecule fluorescence using a gold nanoparticle as an optical nanoantenna. *Phys. Rev. Lett.* **2006**, *97*, 017402. [CrossRef] [PubMed]

31. Kalkbrenner, T.; Håkanson, U.; Sandoghdar, V. Tomographic plasmon spectroscopy of a single gold nanoparticle. *Nano Lett.* **2004**, *4*, 2309–2314. [CrossRef]

32. Lassagne, B.; Garcia-Sanchez, D.; Aguasca, A.; Bachtold, A. Ultrasensitive Mass Sensing with a Nanotube Electromechanical Resonator. *Nano Lett.* **2008**, 3735–3738. [CrossRef] [PubMed]

33. Dai, M.; Eom, K.; Kim, C.W. Nanomechanical mass detection using nonlinear oscillations. *Appl. Phys. Lett.* **2009**, *95*, 203104. [CrossRef]

34. Natsuki, T.; Endo, M. Vibration analysis of embedded carbon nanotubes using wave propagation approach. *J. Appl. Phys.* **2006**, *99*, 034311. [CrossRef]

35. Shi, J.X.; Natsuki, T.; Ni, Q.-Q. Equivalent Young's modulus and thickness of graphene sheets for the continuum mechanical models. *Appl. Phys. Lett.* **2014**, *104*, 223101. [CrossRef]

36. Batra, R.C.; Sears, A. Continuum models of multi-walled carbon nanotubes, Inter. *J. Solids Struct.* **2007**, *44*, 7577–7596. [CrossRef]
37. Li, C.; Chou, T.W. Mass detection using carbon nanotube-based nanomechanical resonators. *Appl. Phys. Lett.* **2004**, *84*, 5246–5248. [CrossRef]
38. Patela, A.M.; Joshib, A.Y. Investigation of double walled carbon nanotubes for mass sensing. *Proc. Technol.* **2014**, *14*, 290–294. [CrossRef]
39. Patel, A.M.; Joshi, A.M. Characterizing the nonlinear behaviour of double walled carbon nanotube based nano mass sensor. *Microsyst. Technol.* **2017**, *23*, 1879–1889. [CrossRef]
40. Shen, Z.B.; Deng, B.; Li, X.F.; Tang, G.J. Vibration of double-walled carbon nanotube-based mass sensor via nonlocal Timoshenko beam theory. *J. Nanotechnol. Eng.* **2012**, *2*, 031003. [CrossRef]
41. Wang, C.M.; Tan, V.B.C.; Zhang, Y.Y. Timoshenko beam model for vibration analysis of multi-walled carbon nanotubes. *J. Sound Vib.* **2006**, *294*, 1060–1072. [CrossRef]
42. Natsuki, T.; Matsuyama, N.; Shi, J.X.; Ni, Q.-Q. Vibration analysis of nanomechanical mass sensor using carbon nanotubes under axial tensile load. *Appl. Phys. A* **2014**, *116*, 1001–1007. [CrossRef]
43. Natsuki, T.; Matsuyama, N.; Ni, Q.-Q. Vibration analysis of carbon nanotube-based resonator using nonlocal elasticity theory. *Appl. Phys. A* **2015**, *120*, 1309–1313. [CrossRef]
44. Coleman, J.N.; Khan, U.; Blau, W.J.; Gun'ko, Y.K. Small but strong: A review of the mechanical properties of carbon nanotube–polymer composites. *Carbon* **2006**, *44*, 1624–1652. [CrossRef]
45. Behera, L.; Chakraverty, S. Recent researches on nonlocal elasticity theory in the vibration of carbon nanotubes using beam models: A Review. *Arch. Comput. Methods Eng.* **2017**, *24*, 481–494. [CrossRef]
46. Binnig, G.; Quate, C.F.; Gerber, C. Atomic force microscope. *Phys. Rev. Lett.* **1986**, *56*, 930–933. [CrossRef] [PubMed]
47. Hafner, J.H.; Cheung, C.-L.; Woolley, A.T.; Lieber, C.M. Structural andfunctional imaging with carbon nanotube AFM probes. *Prog. Biophys. Mol. Biol.* **2001**, *77*, 73–110. [CrossRef]
48. Chen, L.; Cheung, C.-L.; Ashby, P.D.; Lieber, C.M. Single-walled carbon nanotube AFM probes: Optimal imaging resolution of nanoclusters and biomolecules in ambient and fluid environments. *Nano Lett.* **2004**, *4*, 1725–1731. [CrossRef]
49. Hafner, J.H.; Cheung, C.-L.; Oosterkamp, T.H.; Lieber, C.M. High-yield assembly of individual single-walled carbon nanotube tips for scanning probe microscopies. *J. Phys. Chem. B* **2001**, *105*, 743–746. [CrossRef]
50. Dai, H.; Hafner, J.H.; Rinzler, A.G.; Colbert, D.T.; Smalley, R.E. Nanotubes as nanoprobes in scanning probe microscopy. *Nature* **1996**, *384*, 147–150. [CrossRef]
51. Nguyen, C.V.; Stevens, R.M.D.; Barber, J.; Han, J.; Meyyappan, M.; Sanchez, M.I.; Larson, C.; Hinsberg, W.D. Carbon nanotube scanning probe for profiling of deep-ultraviolet and 193 nm photoresist patterns. *Appl. Phys. Lett.* **2002**, *81*, 901–903. [CrossRef]
52. Fang, F.Z.; Xu, Z.W.; Dong, S.; Zhang, G.X. High aspect ratio nanometrology using carbon nanotube probes in atomic force microscopy. *CIRP Ann.-Manuf. Technol.* **2007**, *56*, 533–536. [CrossRef]
53. Sader, J.E.; Sader, R.C. Susceptibility of atomic force microscope cantilevers to lateral forces: Experimental verification. *Appl. Phys. Lett.* **2000**, *83*, 3195–3197. [CrossRef]
54. Hafner, J.H.; Cheung, C.L.; Lieber, C.M. Growth of nanotubes for probe microscopy tips. *Nature* **1999**, *398*, 761–762. [CrossRef]
55. Cheung, C.L.; Hafner, J.H.; Lieber, C.M. Carbon nanotube atomic force microscopy tips: Direct growth by chemical vapor deposition and application to high-resolution imaging. *Proc. Natl. Acad. Sci. USA* **2000**, *97*, 3809–3813. [CrossRef] [PubMed]
56. Liu, C.; Cheng, H.M. Carbon nanotubes: Controlled growth and application. *Mater. Today* **2013**, *16*, 219–228. [CrossRef]
57. Cumings, J.; Zettl, A. Low-Friction nanoscale linear bearing realized from multiwall carbon nanotubes. *Science* **2000**, *289*, 602–604. [CrossRef] [PubMed]
58. Kang, J.W.; Kwon, O.K.; Lee, J.H.; Choi, Y.G.; Hwang, H.J. Frequency change by inter-walled length difference of double-wall carbon nanotube resonator. *Solid State Commun.* **2009**, *149*, 1574–1577. [CrossRef]
59. Zhao, J.; He, M.R.; Dai, S.; Huang, J.Q.; Wei, F.; Zhu, J. TEM observations of buckling and fracture modes for compressed thick multiwall carbon nanotubes. *Carbon* **2011**, *49*, 206–213. [CrossRef]
60. Kuzumaki, T.; Mitsuda, Y. Nanoscale mechanics of carbon nanotube evaluated by nanoprobe manipulation in transmission electron microscope. *Jpn. J. Appl. Phys.* **2006**, *45*, 364–368. [CrossRef]

61. Misra, A.; Tyagi, P.K.; Rai, P.; Mahopatra, D.R.; Ghatak, J.; Satyam, P.V.; Avasthi, D.K.; Misra, D.S. Axial buckling and compressive behavior of nickel-encapsulated multiwalled carbon nanotubes. *Phys. Rev. B* **2007**, *76*, 014108. [CrossRef]

62. Shima, H. Buckling of carbon nanotubes: A state of the art review. *Materials* **2012**, *5*, 47–84. [CrossRef]

63. Shi, J.X.; Natsuki, T.; Lei, X.W.; Ni, Q.-Q. Buckling instability of carbon nanotube AFM probe clamped in an elastic medium. *ASME J. Nanotechnol. Eng. Med.* **2012**, *3*, 020903. [CrossRef]

64. Pantano, A.; Boyce, M.C.; Parks, D.M. Mechanics of axial compression of single-and Multi-wall carbon nanotubes. *ASME J. Eng. Mater. Technol.* **2004**, *126*, 279–284. [CrossRef]

65. Ru, C.Q. Axially compressed buckling of a double walled carbon nanotube embedded in an elastic medium. *J. Mech. Phys. Solids* **2001**, *49*, 1265–1279. [CrossRef]

66. Natsuki, T.; Tsuchiya, T.; Ni, Q.-Q.; Endo, M. Torsional elastic instability of double-walled carbon nanotubes. *Carbon* **2010**, *48*, 4362–4368. [CrossRef]

67. Arroyo, M.; Belytschko, T. Nonlinear mechanical response and rippling of thick multiwalled carbon nanotubes. *Phys. Rev. Lett.* **2003**, *91*, 215505. [CrossRef] [PubMed]

68. Natsuki, T.; Fujita, N.; Ni, Q.-Q.; Endo, M. Buckling properties of carbon nanotubes under hydrostatic pressure. *J. Appl. Phys.* **2009**, *106*, 084310. [CrossRef]

69. Yakobson, B.I.; Brabec, C.J.; Bernholc, J. Nanomechanics of carbon tubes: Instabilities beyond linear response. *Phys. Rev. Lett.* **1996**, *76*, 2511–2514. [CrossRef] [PubMed]

70. Silvestre, N. On the accuracy of shell models for torsional buckling of carbon nanotubes. *Eur. J. Mech.-A/Solids* **2012**, *32*, 103–108. [CrossRef]

71. Hu, Y.G.; Liew, K.M.; Wang, Q.; He, X.Q.; Yakobson, B.I. Nonlocal shell model for elastic wave propagation in single- and double-walled carbon nanotubes. *J. Mech. Phys. Solids* **2008**, *56*, 3475–3485. [CrossRef]

72. Ru, C.Q. Effect of van der Waals forces on axial buckling of a double walled Carbon nanotube. *J. Appl. Phys.* **2000**, *87*, 7227–7231. [CrossRef]

73. Ansari, R.; Rouhi, H. Nonlocal Flugge shell model for the axial buckling of single-walled Carbon nanotubes: An analytical approach. *Int. J. Nano Dimens.* **2015**, *6*, 453–462.

74. He, X.Q.; Kitipornchai, S.; Liew, K.M. Buckling analysis of multiwalled carbon nanotubes: A continuum model accounting for van der Waals interaction. *J. Mech. Phys. Solids* **2005**, *53*, 303–326. [CrossRef]

75. Ru, C.Q. Column buckling of multiwalled carbon nanotubes with interlayer radial displacements. *Phys. Rev. B* **2000**, *62*, 16962–16967. [CrossRef]

76. Zhang, Y.Q.; Liu, X.; Zhao, J.H. Influence of temperature change on column buckling of multiwalled carbon nanotubes. *Phys. Lett. A* **2008**, *372*, 1676–1681. [CrossRef]

77. Natsuki, T.; Ni, Q.Q.; Endo, M. Stability analysis of double-walled carbon nanotubes as AFM probes based on a continuum model. *Carbon* **2011**, *49*, 2532–2537. [CrossRef]

78. Stevens, R.M. New carbon nanotube AFM probe technology. *Mater. Today* **2009**, *12*, 42–45. [CrossRef]

79. Aqel, A.; El-Nour, K.M.M.A.; Ammar, R.A.A.; Al-Warthan, A. Carbon nanotubes, science and technology part (I) structure, synthesis and characterization. *Arabian J. Chem.* **2012**, *5*, 1–23. [CrossRef]